FILLING THE HOLES IN THE SPACE-TIME CUBE OF SNOWPACK EVOLUTION WITH LASERS, CAMERAS, COMPUTERS, AND SNOW SHOVELS

Mark S. Raleigh[1] and Jeffrey S. Deems[1]

ABSTRACT

An information revolution in high-resolution snow observation is producing unprecedented applications in snow research and management of snow-dominated watersheds. Lidar technology has transformed our view and understanding of the spatial nature of snow depth. Between and after lidar flights, sparse in situ measurements are the only direct snowpack data. The central problem is that large gaps in the evolution of snowpack properties through space and time remain even when high-resolution repeat lidar are combined with time-continuous spare point observations. What is needed are additional tools and sources of information to "fill in" the snow data cube. In this project, we assess how time-lapse photogrammetry can help guide modeling decisions and assess model realism. The study focuses on the well-instrumented Senator Beck Basin, a small headwaters basin near Red Mountain Pass, Colorado. Daily maps of binary snow cover and a new dust-on-snow index are derived from a time-lapse camera at a 3 m resolution through the 2013 snowmelt season. A high-resolution (20 meter) snow model is applied using five methods for distributing precipitation spatially, including terrain-based approaches (e.g., lapse rates) and data-driven approaches (e.g., scaled by snow depth patterns from airborne lidar data). The different modeling approaches show a range of structure in spatial snow patterns, with data-driven approaches yielding higher spatial complexity, which are also seen in the camera data. Relative to camera observations, the models tend to estimate higher snow-covered area in the snowmelt season. As suggested by the camera-derived dust indices, this result may be explained by the lack of dust-enhancement in the modeled snowmelt. This study demonstrates the value of time-lapse cameras for identifying strengths and shortcomings of snow models, thereby guiding snow estimation approaches when high resolution snow depth data are unavailable. (KEYWORDS: snow distribution, time-lapse, modeling, dust-on-snow)

INTRODUCTION

The snow hydrology community is recognizing that snowpack patterns and processes are best understood through the integration of multiple datasets, such as from remote sensing, models, and field observations (Raleigh, 2013; Sturm, 2015). The recent Airborne Snow Observatory (ASO) missions have demonstrated the potential for repeat mapping of snow depth at a high spatial resolution (Painter et al., 2016) that when combined with a physical snow density model, can yield detailed snow water equivalent (SWE) datasets for research and operations. ASO is one indicator of a paradigm shift from spatially sparse and temporally infrequent observations (e.g., monthly snow courses at select locations) to more spatially and temporally comprehensive snow datasets. Toward that end, it is essential to reduce uncertainty in snow models, which are necessary to "fill the gaps" in snow information that persist in space and time (e.g., before, between, and after airborne lidar acquisitions) and to improve model realism for snow variables that are not observed directly (e.g., snow density).

Snow accumulation remains a major source of uncertainty for mapping SWE (and snow depth) using snow models (Raleigh et al., 2015), with spatial snow cover patterns being controlled by wind redistribution, microtopography, and vegetation processes (i.e., in forests) at local scales and by elevation-dependent precipitation, freezing level, and melt energy at watershed scales (Clark et al., 2011). There are several approaches available for representing these snow accumulation patterns, but often there is limited guidance about realistic methods and appropriate parameters for a specific application. A variety of measurement techniques have been developed to map SWE via snow depth, which in turn could inform modeling decisions for distributing precipitation and representing snow accumulation processes. However, most techniques have unique tradeoffs between spatiotemporal resolution, cost, and accuracy (Bühler et al., 2015; Kinar & Pomeroy, 2015). A cost-effective approach that could be used to improve representation of modeled snow accumulation patterns is through time-lapse cameras. Time-lapse cameras have been used for a variety of applications in snow hydrology research (e.g., Currier et al., 2017; Garvelmann et al., 2013; Parajka et al., 2012). Of interest is the ability of time-lapse cameras to capture depletion of snow-covered area and information about melt dynamics, which are fundamental features of snowpack evolution (Liston, 1999).

Paper presented Western Snow Conference 2018

[1] Cooperative Institute for Research in Environmental Sciences (CIRES) / National Snow and Ice Data Center (NSIDC) / Western Water Assessment (WWA), University of Colorado, Boulder, 80309, mraleigh@nsidc.org

In this paper, we explore the capability of oblique time lapse imagery for representing snow patterns at high spatial (3 m) and temporal (daily) resolution. We utilize these camera data to compare different modeling approaches for representing spatial variability in snowfall (i.e., precipitation distributions) in a small headwaters catchment in Colorado. The research aims to address the following two questions: (1) What can a time-lapse camera tell us about snow-covered area and snow surface conditions in a small headwaters basin when other high-resolution data are unavailable? (2) How can a time-lapse camera be used in concert with a physically-based snow model to improve the simulation of snow cover patterns?

DATA AND METHODS

Study Area

The study was conducted in the vicinity of the Senator Beck Basin (SBB) in the San Juan Mountains of Colorado. SBB is a small (291 ha) headwaters research basin that has been managed by the Center for Snow and Avalanche Studies (CSAS) since the mid-2000's. The study area includes snow, meteorological and energy balance measurements made at two locations within the basin (subalpine and alpine) and meteorological measurements made at a nearby ridge site outside the basin (Putney Study Plot). Notably, SBB has been the flagship observatory for monitoring dust-on-snow impacts on snowmelt in the Colorado River Basin. In addition, SBB has been included in airborne lidar surveys from ASO over multiple years, including the 2016-2017 NASA SnowEx campaign. More information on basin characteristics, impacts from dust-on-snow, and legacy of data collection are found in other publications (e.g., Painter et al., 2012; Skiles et al., 2012; Landry et al., 2014).

Time-Lapse Imagery and Analysis

In summer 2011, a D200 DSLR time lapse camera was installed at the Putney Study Plot and has been maintained in subsequent years. This camera is aimed across the valley at SBB and has an unobstructed view of approximately 50% of the land area of the basin. With hourly image acquisition during daylight hours, the camera can capture changes in snow cover at a high temporal resolution.

For this study, we focused on images collected during the spring and summer (i.e., March-July) of the 2013 snowmelt season. We first manually identified images with minimal cloudiness and maximum visibility, and then sub-selected to a single image each day based on a consistent solar elevation through the study period. We then aligned the library of images to a reference image, in order to correct for movement in the camera (e.g., due to wind). This involved developing a routine for automatic detection of the color of the sky and identifying the horizon using Sobol edge detection (Dizerens, 2015). This resulted in a binary image (1=horizon, 0 = above or below horizon) corresponding to each daily image. We then used 2D cross correlation to align the images to the reference binary horizon image; this accounted for translation but not rotation/distortion in the images. After all images were aligned, we georectified the image library to a 3 m digital elevation model (from ASO) using the PRACTISE software (Härer et al., 2013), the camera parameters (i.e., focal length = 50 mm, CCD sensor size = 23.6 x 15.8 mm), and a series of 10 manually identified ground control points. We used the embedded routine within PRACTISE for classifying snow cover based on a dynamic threshold in the blue band. Finally, to extract information about darkening of the snow surface (e.g., due to dust deposition), we developed a normalized difference dust index (NDDI) using the red (R) and blue (B) bands:

$$\mathrm{NDDI} = \frac{\mathrm{R}-\mathrm{B}}{\mathrm{R}+\mathrm{B}}$$

where NDDI in theory increases with increasing dust content for a pixel already identified as snow-covered. Dust deposited on the snow tends to have a reddish color in this region, which provides the physical motivation for this index. For visualizing these indices in space, we converted the NDDI to five qualitative classes (less than -4, -4 to -2, -2 to 0, 0 to +2, and +2 to +4) to correspond to a gradient of dust conditions ranging from cleaner to dirtier snow.

An example of the georectification, snow mapping, and dust-on-snow mapping for two dates is shown in Figure 1. The mapped snow cover shows fidelity to the original RGB imagery from the time-lapse camera throughout the season, and this is especially notable during the melt season when complex snow patterns emerge (see 01 June in Figure 1). The NDDI shows snow in the clean to average spectrum during the early snowmelt season (02 April image) but heterogeneous patterns in darker/dustier snow in the late snowmelt season (01 June image).

The NDDI may respond to dust-on-snow (spring 2013 had a high dust concentration, Skiles et al., 2015), but also may reflect areas with shallow snowpack (e.g., areas with underlying substrate influencing surface reflectance).

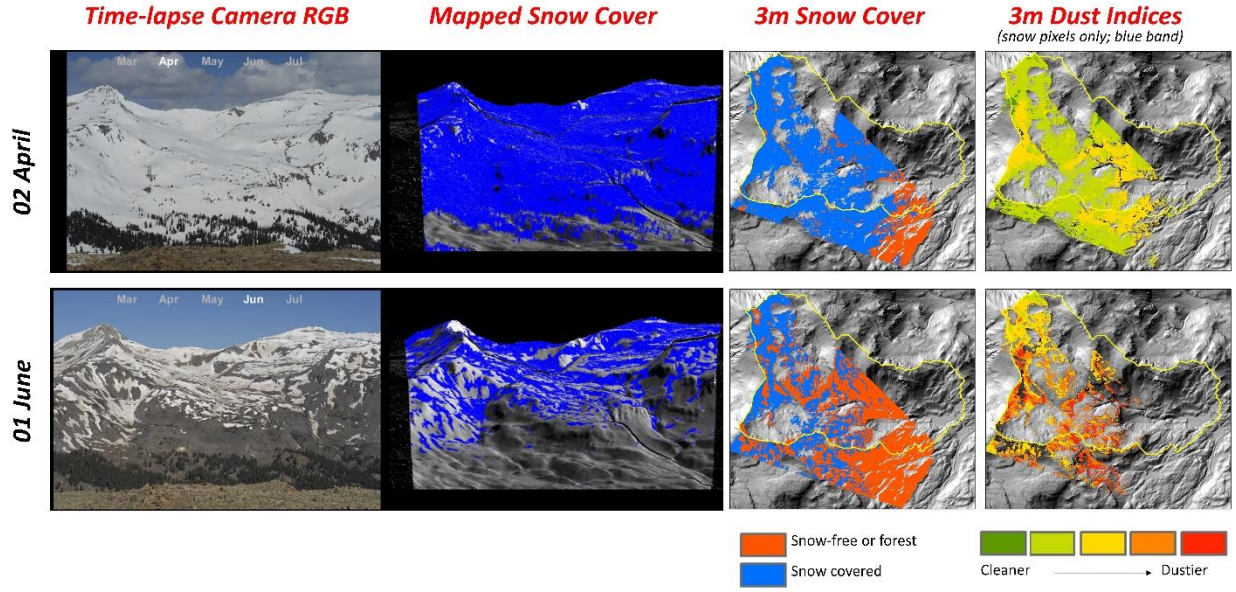

Figure 1. Example RGB images from the time-lapse camera during two dates (April and June) in the 2013 snowmelt season, with corresponding oblique maps of snow cover (second column), orthomaps of snow cover (third column) and NDDI (fourth column). The orthomaps maps (roughly 3 km x 3 km) show an outline of the study basin.

Distributed Snow Modeling

To efficiently represent snow accumulation and melt dynamics in a physically-realistic manner, we applied version 1.0 of the Factorial Snow Model (FSM) (Essery, 2015) using input data distributed at a 20 m spatial resolution over the SBB domain. While FSM is a modular point model that permits systematic testing of model decisions, we did not leverage these capabilities. Instead, we utilized the model configuration with the most detailed process representation and applied that single model over all locations in the basin.

Hourly forcing data were distributed from the subalpine and alpine meteorological stations in the basin using the MeteoIO pre-processor (Bavay & Egger, 2014). Air temperature data were distributed using elevation-detrended ordinary kriging. Relative humidity data were distributed by calculating dew point temperatures at the meteorological stations, interpolating these dewpoint values spatially with an inverse distance weighted lapse rate, and finally calculating relative humidity using air and dew point temperature at each location (Liston & Elder, 2006). Wind fields (speed and direction) were distributed using inverse distance weighted lapse rates and further modified by terrain slope and exposure (Liston & Elder, 2006). Atmospheric loss factors were computed from incoming shortwave radiation data, distributed in space with inverse distance weighting and adjusted for topographic shading to produce spatial estimates of shortwave radiation. Similarly, longwave data were converted to emissivity, distributed using inverse distance weighting, and then converted back to spatially estimate longwave radiation.

Using the time-lapse observations of snow cover, we tested five different approaches for distributing precipitation in MeteoIO for use in FSM. As a base case, we used climatological lapse rates from PRISM (Daly et al., 1994) that account for orographic gradients but not local variations in snow accumulation. Second, we applied the Magnusson et al. (2011) approach that included a lapse rate but also adjusted the precipitation distribution for local slope and curvature (e.g., removing snow from steep slopes and adding snow to concave locations). Third, we used the Winstral et al (2002) method, where precipitation was first distributed using a lapse rate and then modified to account for topographic exposure and sheltering ("default" parameters used, e.g., dmax = 300 m). Fourth, we scaled precipitation based on snow persistence index (SPI) maps computed from Landsat-8 and Sentinel-2 data at 20 m resolution (Wayand et al., 2018). These were normalized by SPI at the precipitation gauge location in the subalpine zone. Finally, we scaled precipitation based on lidar snow depth from an ASO dataset acquired over SBB in a separate year (2017). These five methods provide a range of unique approaches for distributing precipitation. Dynamic methods of precipitation distribution (e.g., a blowing snow model) were not attempted here for simplicity.

RESULTS AND DISCUSSION

Before comparing snow cover patterns from the model to observations from the time-lapse camera (e.g., Figure 1), we first examined spatial patterns in peak SWE from each of the five modeling approaches (Figure 2). The different approaches yielded a range of complexity in spatial structure. Whereas the first three approaches (PRISM, Magnusson, Winstral) revealed spatial patterns broadly linked to topographic factors (e.g., elevation, slopes, wind exposure), the other two methods (SPI and ASO-scaling) revealed more highly complex patterns and more fine-scale variability. The methods had increasing spatial variability as represented by the coefficient of variation (CV, standard deviation divided by the mean SWE). The spatial CV in modeled peak SWE was 0.17 for PRISM, 0.20 for Magnusson, 0.37 for Winstral, 0.46 for SPI, and 0.78 for ASO.

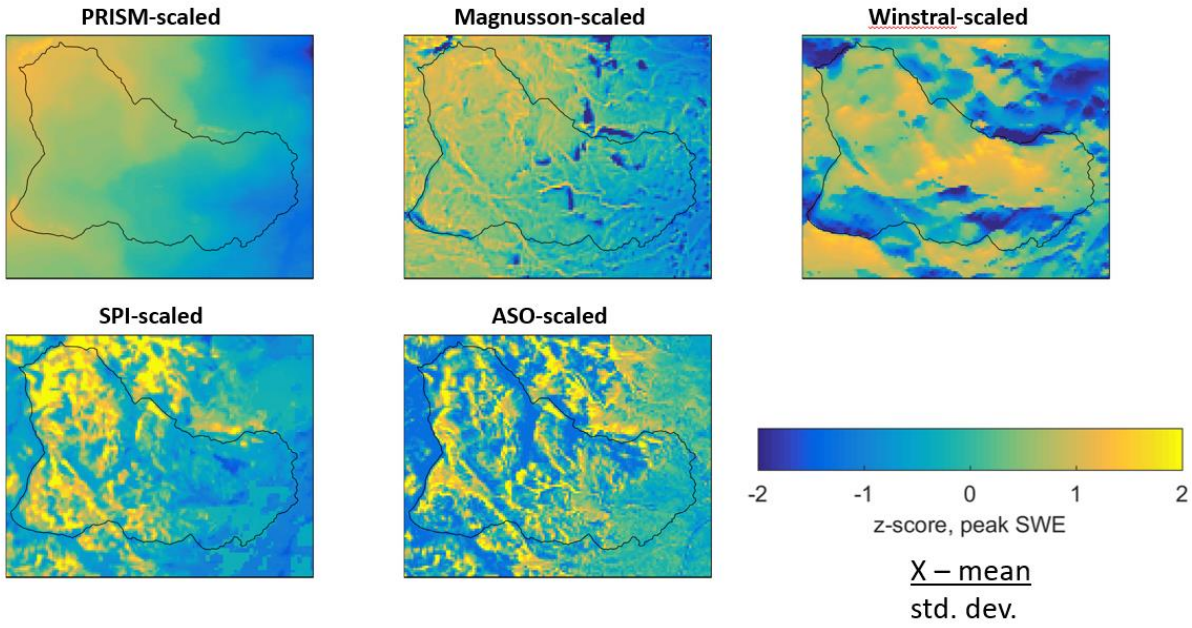

Figure 2. Spatial patterns in normalized peak SWE for the five approaches for distributing precipitation in the model experiment. At each 20 m grid cell, SWE is normalized by removing the mean peak SWE (i.e., average in space) by the standard deviation in peak SWE (i.e., standard deviation in space). Dark blue represents areas of low snow accumulation and yellow represents high snow accumulation. Domain is 2.8 km (E-W) by 2.2 km (N-S).

Spatial patterns in the PRISM and Magnusson methods exhibited controls from prescribed lapse rates (i.e., increasing precipitation and snow accumulation with elevation). These two methods had the highest similarity in peak SWE (Table 1). The Magnusson approach also included enhanced snow accumulation in areas with minimum terrain curvature and reduced accumulation along steeper slopes. The Winstral approach showed more complex patterns in SWE, with zones of reduced or enhanced snow accumulation that reflected the local topography and dominant wind direction. Winstral was not strongly related to any single other method but correlated the most with PRISM and Magnusson (Table 2), likely due to the use of a lapse rate in the background. Patterns in peak SWE were broadly similar between SPI-scaling and ASO-scaling (Figure 2), which were based on remote sensing data, in contrast to other three terrain-based methods. These two approaches had the second greatest correlation (Table 2). Interestingly, SPI had moderate correlations with PRISM (r=0.54) and Magnusson (r=0.56), and ASO (r=0.62), but ASO did not have strong correlations with any of the terrain-based approaches.

Table 1. Correlation matrix for spatial patterns in modeled peak SWE.

	PRISM	**Magnusson**	**Winstral**	**SPI**	**ASO**
PRISM	1	0.85	0.39	0.54	0.10
Magnusson	0.85	1	0.48	0.56	0.18
Winstral	0.39	0.48	1	0.10	0.00
SPI	0.54	0.56	0.10	1	0.62
ASO	0.10	0.18	0.00	0.62	1

Next, we compared snow cover patterns from the five modeling approaches to observations from the time-lapse camera. All approaches showed nearly full snow cover from March to the end of April but began diverging starting in early May. An example of the divergence in spatial snow cover patterns for a date in mid-June is shown in Figure 3. By mid-June, the camera indicated minimal land area covered in snow and heterogeneous snow presence (patchy snow). On this date, the camera indicated only 15% of the viewable domain was snow-covered. In contrast, the models showed 46% snow cover (ASO-scaling), 52% snow cover (SPI-scaling), 73% snow cover (Winstral method), and 80% snow cover (PRISM and Magnusson methods). While none of the model configurations matched the camera snow patterns (Figure 3), the ASO-scaling and SPI-scaling approaches had less spatially continuous snow cover than the PRISM, Magnusson, and Winstral methods (Figure 3). With a few exceptions, the models did not replicate the observed snow patterns. One possible explanation for the discrepancy is that the models did not represent snowmelt patterns realistically, which is plausible given the degradation of albedo due to dust-on-snow (a process not represented in these model simulations). If year-to-year repeatability in snow patterns holds, then we would otherwise have expected methods like ASO-scaling and (to a lesser degree) SPI-scaling to match the observed patterns. Because the camera can only detect spatial patterns in snowpack in the melt season (when deeper areas persist and shallow areas melt out rapidly), the representation of melt effects in the model is also important for comparison with the camera data.

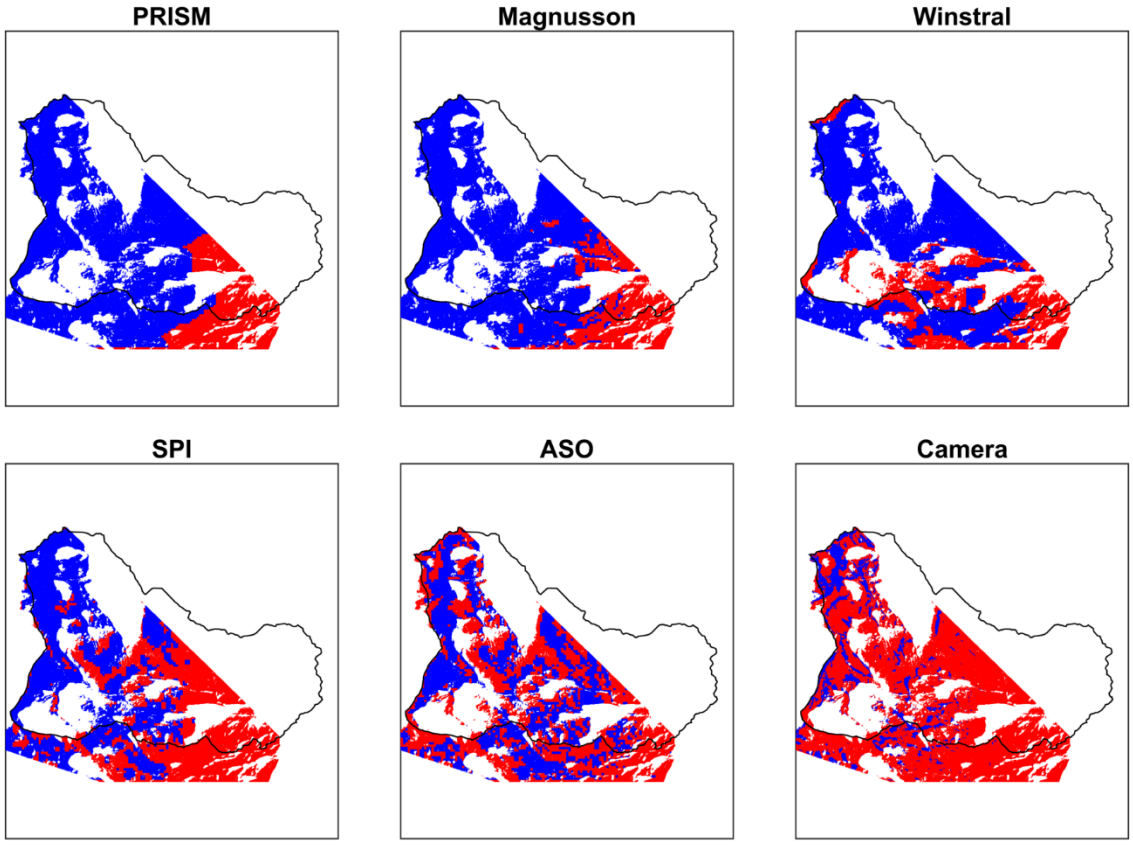

Figure 3. Binary snow cover maps (blue=snow-covered, red = snow free) on 15 June 2013 based on modeled snowpack using five different precipitation distribution schemes (PRISM, Magnusson, Winstral, SPI, and ASO). The observed patterns from the time-lapse camera are also shown. The model simulations (originally at 20 m) are resampled to 3m to match the resolution of the derived snow cover map from the camera. Model grid cells with less than 10 cm snow depth are classified as snow-free while grid cells with 10 cm or deeper snow depth are considered snow-covered. Areas in white are not visible to the camera and are masked out.

To explain the high snow cover in the models (particularly ASO and SPI) and possible influence of dust on snow cover depletion, we examined the progression of domain-averaged fractional snow cover and NDDI through time (Figure 4). The camera results indicate ~90% snow cover (over the camera-viewable area) in March to late April; full snow cover is likely not fully represented in the camera data due to the presence of subalpine forests

(which obscure the camera's oblique view of snow cover) and exposed rock in the camera view. The camera shows snow cover depletion through May and June, with rapid depletion in snow cover in early June. On June 7, the camera showed 12% snow cover in the study domain while model estimates ranged from 55% (ASO-scaling) to 85% (PRISM and Magnusson); this was the largest difference in snow-covered area from the camera versus models at any point in this study period. The days and weeks prior to this date had relatively higher dust indices (Figure 4 bottom) and visible darkening of the snow surface, suggesting that dust-enhanced snowmelt (not represented in the models) was the reason for the more rapid declines in observed snow relative to the modeled snow cover. A snow storm on 8 June temporarily decreased the dust indices derived from the camera imagery and increased the fractional snow-covered observed by the camera, thereby reducing differences between observed and modeled snow cover. In the second half of June, the observed snow fraction dropped below 10% and diminished to 0% by mid-July; dust-indices gradually increased during this period (Figure 4), reflecting retention of dust on late-lying snow drifts and/or exposed vegetation/substrate in shallow, persistent snow.

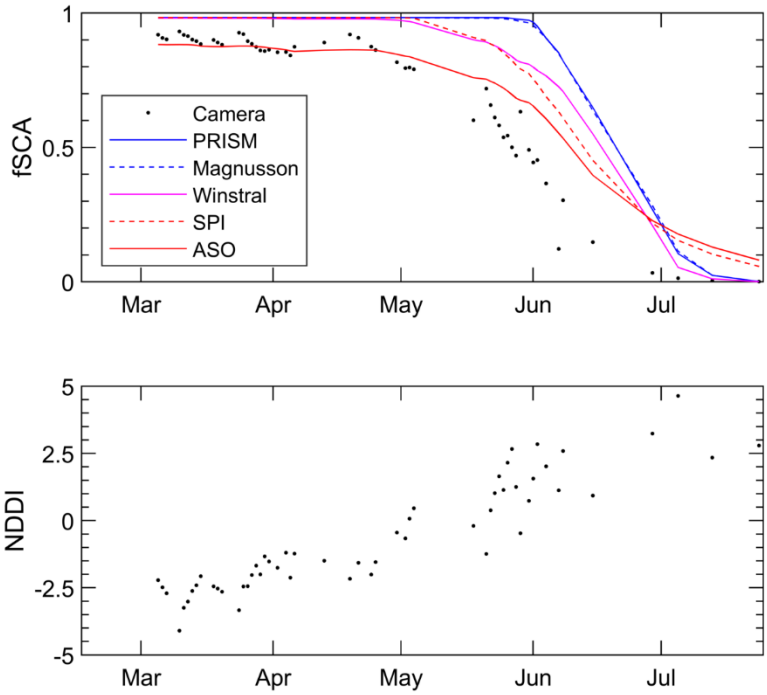

Figure 4. (top) Time series of fractional snow-covered area (fSCA) for camera-viewable area only in the study domain during the 2013 snowmelt season as represented by the time-lapse camera and five snow models with different precipitation distribution approaches. (bottom) Time series of domain-averaged normalized difference dust indices (NDDI) mapped only with pixels identified as snow-covered from the time-lapse camera. The general increase in NDDI reflects decreasing albedo due to natural processes (e.g., grain growth) but also dust deposition. The seasonal increase in NDDI is punctuated by intermittent snow events that reset surface albedo and thus decrease the dust indices for short intervals (e.g., two snow events in second half of May cause short-term decrease in NDDI).

CONCLUSIONS

Monitoring snow-covered area and surface reflectance (as approximated by the dust-indices) from a time-lapse camera provides a cost-effective and reliable means of obtaining high-resolution, daily snow information that can help fill gaps in snowpack monitoring. Specifically, a camera provides a benchmark for discriminating the relative realism of different approaches for distributing precipitation spatially, and for identifying deficiencies in modeled processes like snowmelt (in this case, enhanced by dust). Modeled snow patterns based on precipitation scaled from ASO lidar snow depth and satellite-observed snow persistence indices (SPI) best matched patterns found in the time-lapse imagery but did not replicate the exact patterns or fraction of snow cover observed by the camera. At the scale of a headwaters basin in a continental climate, the more simplistic modeling approaches for distributing precipitation (e.g., a specified lapse rate) were not realistic (as seen here when the model used PRISM lapse rates).

Future work could build on this effort by examining snow patterns from a more sophisticated model that more explicitly represents snow redistribution processes (Alpine3D or SnowTrans3D), by directly assimilating the camera-derived snow-covered area, and by including modeling approaches that account for dust-enhancement of snowmelt (e.g., via data assimilation of surface reflectance data). The dust effect might be mitigated by examining a range of years with varying levels of dust conditions. For example, 2015 had minimal dust impacts in Senator Beck Basin and might provide a cleaner test of how models represent spatial patterns in snow accumulation. Identification of models that portray realistic snow distributions adds value to spatial snow depth surveys (e.g., airborne lidar) and has the potential for more robust quantification of snowpack during periods without intensive snow sampling.

ACKNOWLEDGMENTS

This work was supported by a 2017-2018 CIRES Innovative Research Project grant (J. Deems as PI), hosted at the National Snow and Ice Data Center. The authors thank CIRES for the opportunity to conduct this work under IRP support. We would like to thank the Center for Snow and Avalanche Studies for data collection and support in the Senator Beck Basin. We also thank the NASA JPL Airborne Snow Observatory (ASO) team for providing lidar snow depth data over the basin. Finally, we thank Nic Wayand for providing code in Google Earth Engine to compute the snow persistence metrics from Landsat 8 and Sentinel 2 data.

REFERENCES

Bavay M. and T. Egger. 2014. MeteoIO 2.4.2: a preprocessing library for meteorological data. *Geoscientific Model Development,* **7**, 3135–3151.

Bühler Y., M. Marty, L. Egli, J. Veitinger, T. Jonas, P. Thee, and C. Ginzler. 2015. Snow depth mapping in high-alpine catchments using digital photogrammetry. *The Cryosphere*, **9**, 229–243.

Clark M.P., J. Hendrikx, A.G. Slater, D. Kavetski, B. Anderson, N.J. Cullen, T. Kerr *et al.* 2011. Representing spatial variability of snow water equivalent in hydrologic and land-surface models: A review. *Water Resources Research,* **47**, W07539.

Currier W.R., T. Thorson, and J.D. Lundquist. 2017. Independent Evaluation of Frozen Precipitation from WRF and PRISM in the Olympic Mountains. *Journal of Hydrometeorology*, **18**, 2681–2703.

Daly C., R.P. Neilson, and D.L. Phillips. 1994. A statistical–topographic model for mapping climatological precipitation over mountainous terrain. *J. Appl. Meteorol.*, **33**, 140–158.

Dizerens C. 2015. Georectification and snow classification of webcam images : potential for complementing satellite-derrived snow maps over Switzerland. M.S. thesis, University of Bern.

Essery R. 2015. A factorial snowpack model (FSM 1.0). *Geoscientific Model Development*, **8**, 3867–3876.

Garvelmann J., S. Pohl, and M. Weiler. 2013. From observation to the quantification of snow processes with a time-lapse camera network. *Hydrology and Earth System Sciences*, **17**, 1415–1429.

Härer S., M. Bernhardt, J.G. Corripio, and K. Schulz. 2013. PRACTISE – Photo Rectification And ClassificaTIon SoftwarE (V.1.0). *Geoscientific Model Development*, **6**, 837–848.

Kinar N.J. and J.W. Pomeroy. 2015. Measurement of the physical properties of the snowpack. *Reviews of Geophysics*, **53**, 481–544.

Landry C.C., K.A. Buck, M.S. Raleigh, and M.P. Clark. 2014. Mountain system monitoring at Senator Beck Basin, San Juan Mountains, Colorado: A new integrative data source to develop and evaluate models of snow and hydrologic processes. *Water Resources Research*, **50**, 1773–1788.

Liston G.E. 1999. Interrelationships among Snow Distribution, Snowmelt, and Snow Cover Depletion:

Implications for Atmospheric, Hydrologic, and Ecologic Modeling. *Journal of Applied Meteorology*, **38**, 1474–1487.

Liston G.E. and K. Elder. 2006. A Meteorological Distribution System for High-Resolution Terrestrial Modeling (MicroMet). *Journal of Hydrometeorology*, **7**, 217–234.

Magnusson J., D. Farinotti, T. Jonas, and M. Bavay. 2011. Quantitative evaluation of different hydrological modelling approaches in a partly glacierized Swiss watershed. *Hydrological Processes*, **25**, 2071–2084.

Painter T.H., D.F. Berisford, J.W. Boardman, K.J. Bormann, J.S. Deems, F. Gehrke, A. Hedrick *et al.* 2016. The Airborne Snow Observatory: Fusion of scanning lidar, imaging spectrometer, and physically-based modeling for mapping snow water equivalent and snow albedo. *Remote Sensing of Environment*, **184**, 139–152.

Painter T.H., S.M. Skiles, J.S. Deems, A.C. Bryant, and C.C. Landry. 2012. Dust radiative forcing in snow of the Upper Colorado River Basin: 1. A 6 year record of energy balance, radiation, and dust concentrations. *Water Resources Research*, **48**, W07521.

Parajka J., P. Haas, R. Kirnbauer, J. Jansa, and G. Blöschl. 2012. Potential of time-lapse photography of snow for hydrological purposes at the small catchment scale. *Hydrological Processes*, **26**, 3327–3337.

Raleigh M.S. 2013. Quantification of uncertainties in snow accumulation, snowmelt, and snow disappearance dates. Ph.D. dissertation, University of Washington.

Raleigh M.S., J.D. Lundquist, and M.P. Clark. 2015. Exploring the impact of forcing error characteristics on physically based snow simulations within a global sensitivity analysis framework. *Hydrology and Earth System Sciences*, **19**, 3153–3179.

Skiles S.M., T.H. Painter, J.S. Deems, A.C. Bryant, and C.C. Landry. 2012. Dust radiative forcing in snow of the Upper Colorado River Basin: 2. Interannual variability in radiative forcing and snowmelt rates. *Water Resources Research*, **48**, W07522.

Skiles S.M., T.H. Painter, J. Belnap, L. Holland, R.L. Reynolds, H.L. Goldstein, and J. Lin. 2015. Regional variability in dust-on-snow processes and impacts in the Upper Colorado River Basin. *Hydrological Processes*, **29**, 5397–5413.

Sturm M. 2015. White water: Fifty years of snow research in WRR and the outlook for the future. *Water Resources Research*, **51**.

Wayand N.E., C.B. Marsh, J.M. Shea, and J.W. Pomeroy. 2018. Globally scalable alpine snow metrics. *Remote Sensing of Environment*, **213**, 61–72.

Winstral A., K. Elder, and R. Davis. 2002. Spatial snow modeling of wind-redistributed snow using terrain-based parameters. *Journal of Hydrometeorology*, **3**, 524–538.